communications earth & environment

Article

https://doi.org/10.1038/s43247-024-01246-5

Maximum tree height in European Mountains decreases above a climate-related elevation threshold

P. J. Gelabert[1,2] ✉, M. Rodrigues[3,4], L. Coll[1,2], C. Vega-Garcia[1,2] & A. Ameztegui[1,2]

Mountain forests face important threats from global change and spatio-temporal variation in tree height can help to monitor these effects. In this study, we used the Global Ecosystem Dynamics Investigation space-borne laser sensor to examine the relationship between maximum tree height and elevation, and the role of climate, in the main European mountain ranges. We found a piecewise relationship between elevation and maximum tree height in all mountain ranges, supporting the existence of a common breakpoint that marks the beginning of tree development limitations. Temperature and precipitation were identified as the most important drivers of tree height variation. Additionally, we predicted significant upward displacement of the breakpoint for the period 2080-2100 under climate change scenarios, potentially increasing the area without growth limitations for trees. These findings contribute to understanding the impacts of global warming on mountain forest ecosystems and provide insights for their monitoring and management.

Mountain forests account for 23% of the forested lands worldwide and sustain about half of the world's population[1]. They provide a wide array of goods and services, such as timber, shelter from animals, air purification, and carbon sequestration. However, their persistence and ability to provide ecosystem services, including the provision of timber and non-timber forest products[2], are seriously threatened by the advent of global change[3]. It is, therefore, essential to design and adopt the required adaptation strategies.

Tree height is a good indicator of biological productivity and site quality[4] and has recently been used to produce continuous estimates of aboveground biomass and carbon storage[5,6]. Additionally, tree height is a proxy for ecosystem structure, with its heterogeneity being an essential variable for predicting species richness at different scales[7,8]. Furthermore, monitoring tree height can aid in anticipating the effects of global change on forest ecosystems[4].

On a global scale, the determination of maximum tree height is shaped by the convergence of environmental factors and historical land use legacies[9]. Existing research consistently points to a positive association between maximum canopy height and the stability of past climatic conditions[9]. Additionally, tree height is shaped by the combined effects of water and energy availability[10]. The relative significance of these two components varies along latitudinal gradients, with greater energy constraints observed in boreal forests and an increasingly pronounced water limitation in lower latitudes[9]. Moreover, the transformation of forested landscapes influenced by land use legacies has played a role in diminishing the stature of forest canopies over time[11,12]. Specifically, in the European mountainous regions, climate mainly drives tree development[13–16]. In summary, temperature emerges as the primary limiting factor for maximum tree height at high elevations, while water availability predominantly influences tree development in lowland areas[13,16,17]. Nonetheless, microclimate also plays a key role in mountain forest development[18], and soil moisture and nutrient availability have a role at the local scale[19].

Tree height is often analyzed at the local scale through field-based forest inventories[20], which are expensive, time-consuming and limited in extent. Recently, active remote sensing methods, and particularly the use of LiDAR sensors, have been used to produce accurate and dense samplings of forest structures at large spatial extents[21], overcoming optical data limitations[22]. However, airborne LiDAR is characterized by its elevated acquisition costs, unpredictable procurement timelines and limited spatial coverage[23]. Additionally, wall-to-wall initiatives face inherent limitations tied to government funding and prioritization. In this regard, space-borne laser sensors, such as Global Ecosystem Dynamics Investigation (GEDI) can overcome the aforementioned limitations and offer a unique solution for tree height

[1]Department of Agricultural and Forest Sciences and Engineering (DCEFA), Universitat de Lleida, Alcalde Rovira Roure 191, 25198 Lleida, Catalonia, Spain. [2]Joint Research Unit CTFC-Agrotecnio-Cerca, Ctra. Sant Llorenç Km.2, 25280 Solsona, Catalonia, Spain. [3]Department of Geography, University of Zaragoza, Pedro Cerbuna 12, 50009 Zaragoza, Aragón, Spain. [4]GEOFOREST Research Group, University Institute for Environmental Sciences (IUCA), Zaragoza, Spain.
✉e-mail: perejoan.gelabert@udl.cat

sampling at a global scale. Nonetheless, these data sources should be used with caution and considering their limitations and challenges, such as the footprint elongation that GEDI is known to present in steep slopes[24].

In a recent study leveraging airborne LiDAR, we reported non-linear relations between elevation and maximum tree height in the Pyrenees[25]. In particular, we found a piecewise response of maximum tree height, with a sharp downward profile above a certain elevation threshold or breakpoint[25,26]. These results showed the existence of region-wide patterns in maximum tree height decline with elevation but whether this piecewise pattern is prevalent in other mountain regions has not yet been confirmed. In this work, we use the GEDI full-waveform space-borne laser instrument to investigate the relationship between maximum tree height and elevation, temperature, and rainfall for the main European mountainous ranges. GEDI is the first active remote sensing laser sensor onboard the International Space Station tailored to provide detailed 3D information about forest structure and responses at the regional/global level. The GEDI program offers global coverage between 51.6°S-51.6°N latitudes, demonstrating strong performance in characterizing mountain forest ecosystems at the landscape level[27], making it ideal for evaluating the generality of patterns and processes.

Our main objectives were (i) to ascertain whether the existence of a 'breakpoint' in the response of maximum tree height to elevation holds over the main European mountain ranges; (ii) to identify the climatic drivers of variations in maximum tree height across mountain ranges; and (iii) to foresee the displacement of the breakpoint under different climate change scenarios. We hypothesize that the breakpoint observed in the Pyrenees holds over the main European mountain ranges, making it a useful indicator to monitor the early impacts of global warming on mountain forest ecosystems.

Results

Maximum tree-height decrease in elevation follows a non-linear profile

We observed a non-linear response in the elevation-maximum tree height relationship across the main European mountain systems. The data supported the existence of a unique breakpoint in all mountain ranges but the elevation where it appeared varied across mountain ranges (Fig. 1). The Caucasus (1740.2 ± 3.9 m.a.s.l.) displayed the tipping point at higher elevations than the Pyrenees (1490.9 ± 5.7 m.a.s.l.), the Alps (1474.3 ± 10.8 m.a.s.l.) and the Carpathians (1416.2 ± 7.0 m.a.s.l.). Above this breakpoint, maximum tree height declined faster in Eastern Mountain ranges – Carpathians, −3.31 m/100 m; Caucasus −2.28 m/100 m—compared to mountain ranges under greater oceanic influence—Alps, −1.4 m/100 m; Pyrenees, −1.24 m/100 m. Non-linear modeling

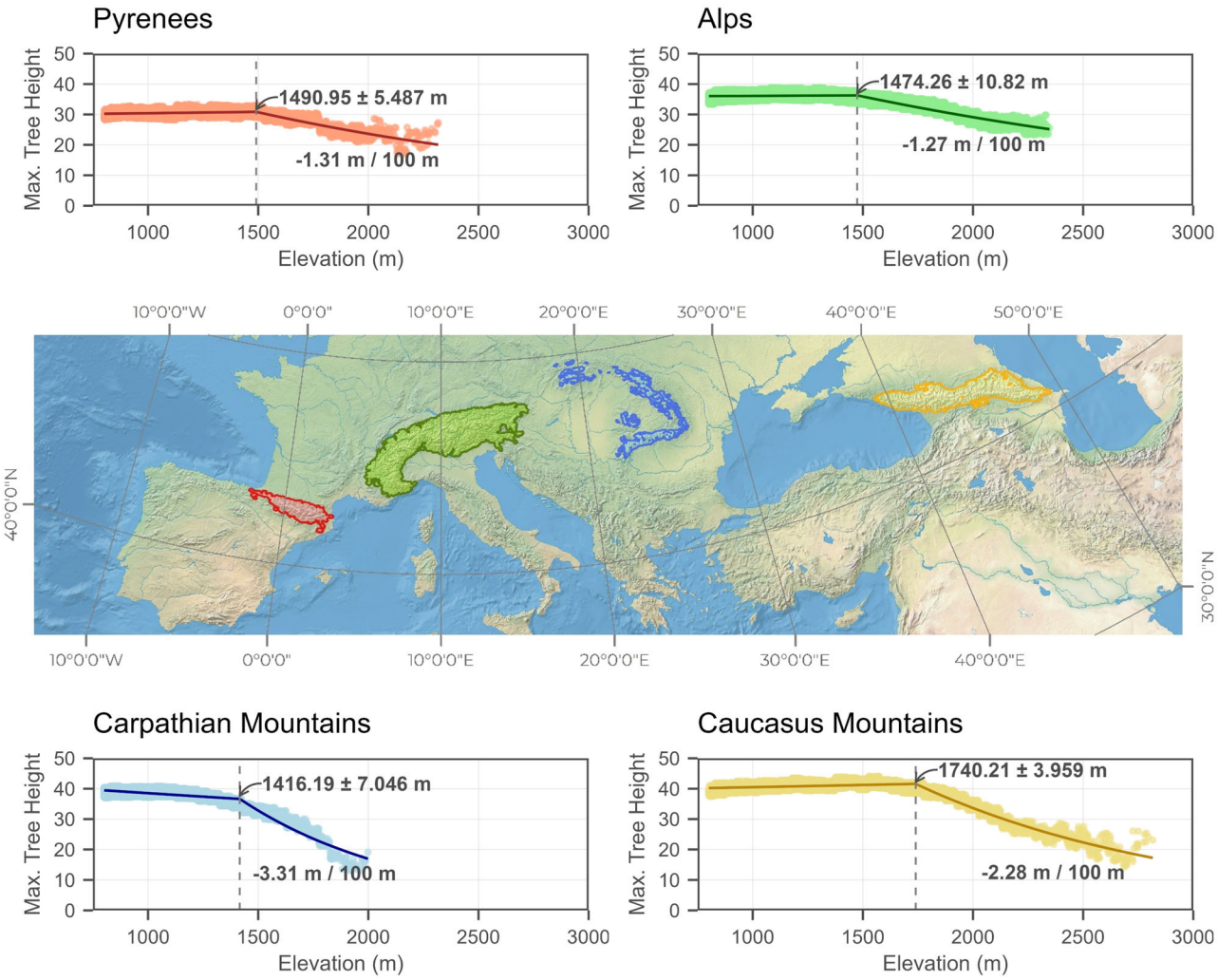

Fig. 1 | Variation in maximum tree height with elevation in the four analyzed mountain ranges. Alps (green), Pyrenees (red), Caucasus Mountains (yellow) and Carpathian (blue). Solid colored lines display the predicted relationship between elevation and maximum tree height, based on the bootstrapped median of model parameters; points represent GEDI observed tree heights between the 90th and 95th percentiles. Vertical dashed lines mark the average estimated position of the breakpoint (with its corresponding value ± standard deviation indicated in numbers) across the 1000 bootstrap models. Values below the solid lines report the slope of the relationship profile beyond the breakpoint. Natural earth's relief base map in the background.

Table 1 | Summary of model performance.

		R^2					
	Model	**Elev**	$T_{MeanMaxSummer}$	$T_{MeanMinGS}$	**LGS**	$Prec_{AccAnnual}$	$Prec_{AccSummer}$
Alps	Linear	0.53	0.01	0.06	0	0.09	0.41
	Segmented	0.78	0.81	0.72	0.82	0.24	0.76
	Gaussian	0.8	0.81	0.7	0.76	0.14	0.73
Pyrenees	Linear	0.4	0.09	0.02	0.05	0.28	0.41
	Segmented	0.71	0.85	0.58	0.5	0.85	NA
	Gaussian	0.68	NA	0.42	0.36	0.81	NA
Carpathian	Linear	0.58	0.55	0.64	0.58	NA	0.43
	Segmented	0.85	0.85	0.83	0.86	NA	0.44
	Gaussian	0.88	0.85	0.87	0.88	0.36	0.45
Caucasus	Linear	0.46	0.27	0.07	0.4	0.23	0.26
	Segmented	0.92	0.9	0.74	0.9	NA	0.36
	Gaussian	0.9	0.88	0.75	0.85	NA	0.44

NA values represent models that performed best with a non-segmented pattern or where segmented and Gaussian models were not applicable. *R2* Coefficient of determination, *Elev* elevation, $T_{MeanMaxSummer}$ mean of summer maximum temperature, $T_{MeanMinGS}$ mean of minimum temperatures in the growing season, *LGS* length of the growing season (no. of days), $Prec_{AccAnnual}$ annual accumulated precipitation, $Prec_{AccSummer}$ Summer accumulated precipitation.

alternatives outperformed the linear regression baseline in all mountain ranges (Table 1 and Table SI 1) with both a Gaussian and a segmented model providing a similar fit ($R^2 > 0.74$).

Drivers of the decrease of maximum tree height with elevation

Models predicting maximum tree height from elevation were generally as good as the best model using climatic covariates, if not better (Table 1 and Table SI 1). For all the analyzed mountain ranges, temperature variables, specifically $T_{MeanMaxSummer}$ and LGS, were the best climatic predictors of maximum tree height variation. However, for the Pyrenees and Alps Mountains, annual precipitation emerged as a highly influential factor (Table 1). Non-linear relationships were observed for all climate factors, with strong evidence of piecewise trends and the existence of breakpoints, except for summer precipitation in the Pyrenees, as well as for annual precipitation in the Caucasus and Carpathian Mountains, where the data patterns did not support segmentation (Table 1). However, the elevation breakpoint consistently correlated with either temperature, precipitation, or both. In fact, the altitudinal distribution of the temperature-derived breakpoint closely mirrored the values of the elevation-derived breakpoint, consistently falling within the interquartile range of the former. The same happened with precipitation, with the exception of the Caucasus Mountains (Fig. 2).

Climate change effects on the breakpoint position

All the considered climate change models and scenarios foresee an increase in temperature. Since tree height is closely tied to temperature, we expect a general upward shift in the elevational position of the breakpoints by the end of the century, tracking the increases in temperature predicted by all the scenarios. Under the Shared Socioeconomic Pathway 245, the upward displacement of the breakpoint would result in a 60–65% increase in the area where tree height growth is not limited by temperature. In contrast, the area without growth limitations under SSP585 increased between 70% and 100%, consistently reaching the current position of the treeline. The general trend described above was not observed for the Carpathians Mountains, where the estimated breakpoint is already quite close to the current tree line. Consequently, we estimated little further expansion of the non-limited growth area (Fig. 3).

Discussion

Maximum tree height exhibited a clear non-linear response along the elevation gradient in the four mountain ranges analyzed, supporting the existence of a common pattern in controlling the height development of tree vegetation. The non-linear, segmented trend allows the detection of an explicit breakpoint above which maximum tree height starts to decrease linearly with elevation. This breakpoint reflects the climatic limit beyond which the suitability for vegetation growth gradually decreases[25]. We recognize that elevation acts here as a proxy for climate variability, which is the real driver of the observed differences in tree height development. However, the uneven and sparse distribution of stations feeding climate interpolation models such as WorldClim[28] and their low spatial accuracy hinder their reliability in mountain areas[15,29]. Despite drawbacks, the high correlation of climate variables with elevation and the global availability of topographic data makes the latter a suitable variable for monitoring the effects of climate change in mountain areas. Given the slim differences in performance between segmented and Gaussian models, we retained the segmented approach due to its ability to simplify the link into piecewise relationships and breakpoint thresholds. Besides, it facilitates further investigation into the strength of tree height decrease along the elevation gradient.

In three out of the four analyzed mountain ranges (Alps, Carpathian and Caucasus Mountains), the decrease in maximum tree height with elevation was primarily due to thermal limitations, as shown in Table 1. Numerous studies have pointed out the limitation to tree development caused by temperature[14,15,30], particularly in mountain ecosystems and at high latitudes[15]. The strongest evidence of this phenomenon is the existence of the treeline, defined as the elevation limit of arboreal growth form[31]. However, we proved that such thermal limitation begins at much lower elevations[9,25] and our results contribute to identifying the elevation threshold where these processes start in different mountain ranges[9,25]. Nevertheless, in mountainous environments, tree height can also be constrained by effects from wind, snow loads and soil quality, especially at local scales and higher elevations[32–34]. In contrast to the other mountain ranges, maximum tree height development in the Pyrenees seems to be more influenced by precipitation than by thermal limitations. Due to its proximity to the Mediterranean Sea and its west-east disposition, a large part of the Pyrenees features a Mediterranean-type climate characterized by a marked summer drought period, especially on the southern slopes. Even when precipitation was the main driver of maximum tree height development, elevation was still a good estimator of the breakpoint, suggesting it could be used globally as an indicator of the relationship between climate and tree height development[17,25,35]; always considering latitudinal bias corrections[15] and other tree height modulators such as the mass elevation effect, continentality, microtopography and soil development[14,34,36].

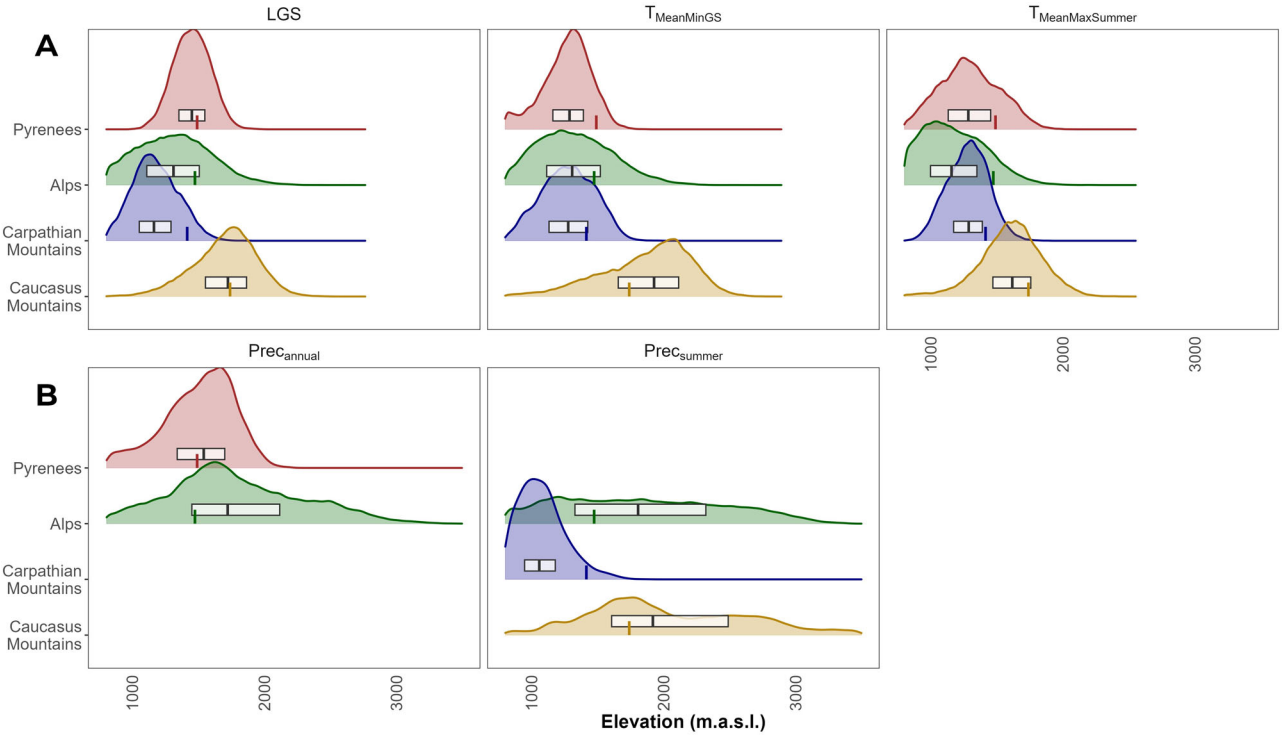

Fig. 2 | Elevation breakpoint climate variable relationship. Densities and violins plots depict the elevation values intersected by **A** isotherm and **B** isohyet defined at breakpoint of maximum tree height-temperature or maximum tree height-precipitation variables in each mountain range. Vertical lines represent the breakpoint of the relation maximum tree height-elevation at each mountain range, and boxplots show the interquartile range and median. No represented data in the plots correspond to non-segmented patterns of the data.

A shift of the optimal growing conditions towards higher elevations is expected in response to global warming[37] (Fig. 3). Furthermore, warming trends are expected to extend the vegetative season, fostering tree growth in the future[38]. Our results predict an upward shift of the breakpoint, oftentimes reaching the current treeline, which would imply the lifting of climatic restrictions on the development of trees. As observed in boreal forests[39–41], the upward displacement of such elevation points may imply a substantial increase in the productivity of these cold-limited forests[42]. Nevertheless, under the most extreme scenarios, the positive effects of climate change could be outweighed by the negative impact of hydric limitations in the most xeric environments[43]. The enhanced development of these "new" forest communities may increase the provision of ecosystem services such as timber and carbon sequestration but simultaneously entail a decrease in open habitats, impacting the associated biodiversity[44,45]. Although upward shifts in the position of the treeline have already been observed as a response to global warming[46], the displacement is far from being universal due to the complexity of factors and nuances influencing the natural afforestation of treeless areas at the limit of their physiological tolerance[14,26]. The maximum height-elevation breakpoint, however, is more likely to relocate, as it indicates a physiological relationship between tree development and climate, not an actual physical limit. This may cause a mismatch between the upward shift of the breakpoint and that of the treeline, with potential consequences for the responses of alpine ecosystems to global change.

Finally, while GEDI has proven its capability to characterize mountain forest structures at the landscape and regional scale[27,47], it is essential to consider certain critical factors when using GEDI data for ecological applications in such environments. Notably, tree height estimations display biases primarily driven by slope-related effects and geolocation accuracy[27]. Despite having the smallest footprint among space-borne LiDAR systems, GEDI cannot fully compensate for footprint elongation due to varying terrain slopes[24]. Additionally, the expected geolocation error of 10 meters can contribute to over 50% of the uncertainty in GEDI-derived height metrics[48,49]. Furthermore, our familiarity with the region suggests that tree heights can be overestimated in this study despite the filters we applied to minimize this effect (see methods). This emphasizes the importance of cautious interpretation when utilizing GEDI data in mountainous forest ecosystems, as has been warned elsewhere[50]. However, our analyses and the comparison with airborne LiDAR data available in the Pyrenees suggest that this overestimation is systematic and does not affect the trends and patterns observed here.

Methods

Study area

Our study area was restricted by the latitudinal scanning range of GEDI (51.6 °S–51.6°N). For this reason, we focused the analyses on the main European mountain ranges within GEDI's reach, concretely the Pyrenees, Alps, Carpathians, and Caucasus. Following the FAO global ecological zoning, we set the lower elevation limit of the analyzed mountain forests at 800 m[51].

The Pyrenees are located along the Spain-France border, within longitudes 2.38°W–3.15°E and latitudes 42.23°N–43.03°N. The highest summits reach ~3400 m above sea level. The lower elevations are dominated by a Mediterranean climate, with an average annual temperature ~8 °C and annual rainfall circa 800 mm, characterized by summer drought on the southern slopes. Higher elevations transition into high mountain climate, with mild temperatures and rainfall over 2500 mm, the wettest among the analyzed areas. Dominant tree species include Scots pine (*Pinus sylvestris L.*), beech (*Fagus sylvatica L.*), silver fir (*Albies alba Mill.*) and mountain pine (*Pinus uncinata* Ram ex. DC).

The Alps constitute the natural border between Italy, Switzerland France, Slovenia, and Austria (5.12°E–16.1°E and 45.52°N–47.62°N), reaching ~4800 m at their highest summit. Climatically diverse, the Alps exhibit uneven annual precipitation ranging from 2300 mm near the Adriatic Sea to 800 mm in the central Alps. The mountain forests of the Alps are characterized by a complex mosaic of mixed coniferous forests. The main species are spruce (*Picea abies* L. Karst.), silver fir, beech, and a variety of pines.

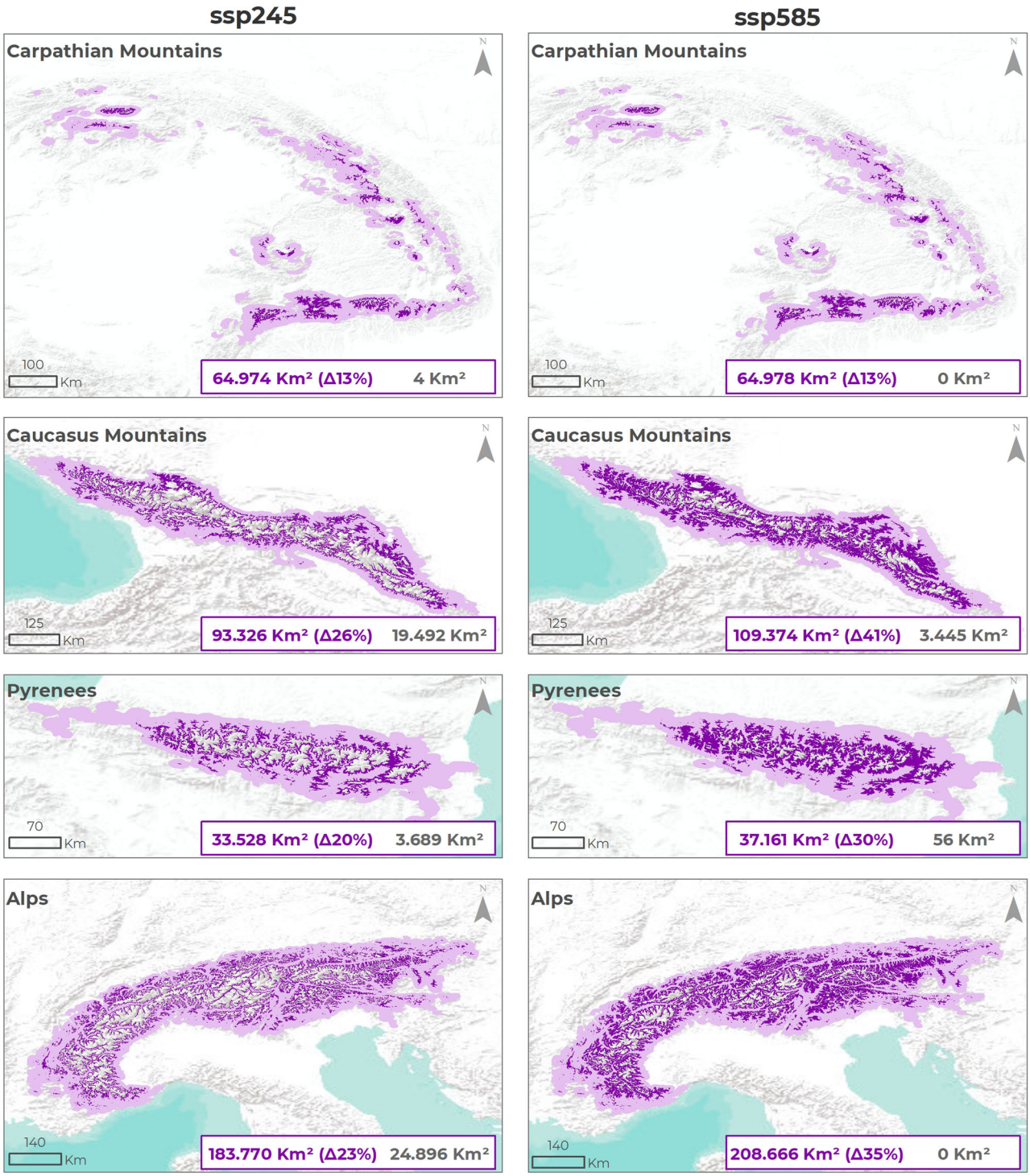

Fig. 3 | Current and future areas without height growth thermal restrictions. Light purple areas represent the areas without growth restrictions under current conditions, while dark purple areas represent the projected areas without growth restrictions by 2100. Numeric values summarize the total area without growth restrictions for the period 2081–2100; values in brackets report the percentage increase in unrestricted area compared to current values; gray values refer to the area with restrictions, defined as the remaining area between the breakpoint in 2100 and the current treeline. Esri hillside is used as a backdrop.

The Carpathians, the most continental mountain range among those analyzed here, cross part of northern Serbia, central Romania, eastern Ukraine, southern Poland, western Czech Republic, northern Hungary, and an important part of Slovakia (18.43°E–26.71°E and 44.73°N–49.1°N). With peaks reaching 2650 m, the Carpathians exhibit. average yearly temperatures ranging from 7 °C at the lowest altitudes to 0 °C at the highest peaks. Annual rainfall varies from i1,400 mm in the northern end to 500 mm in the centre of Romania. The dominant tree species are sycamore (*Acer pseudoplatanus* L.), beech, silver fir, and spruce (*Picea abies*).

The Caucasus Mountains form the natural border between Georgia and Azerbaijan from Russia (39.13°E–49.37°E and 41.74°N–43.13°N). They constitute the largest mountain range analyzed in terms of area and elevation, exceeding 5500 m at the highest summits. At lower elevations, beech (*Fagus orientalis* Lipsky) and various *Quercus* species predominate, while

higher elevations are dominated by spruce (*Picea orientalis* L. Peterm.), fir (*Abies nordmanniana* Spach.) and diverse pine species. The Caucasus Mountains represent the most arid mountain system analyzed, with temperatures above 10 °C and precipitation of about 600 mm in lower elevations. At higher elevations, low temperatures predominate, with an annual average of about 0 °C, and precipitation of ~1000 mm.

GEDI dataset

We used the Global Ecosystem Dynamics Investigation (GEDI) dataset, collected between May 2019 and September 2020[52]. GEDI is a space-borne, high-resolution laser ranging scanner aboard the International Space Station, designed to capture the vertical structure of the canopy layer across temperate and tropical forests (between 51.6° latitude, northern and southern hemisphere)[53]. GEDI consists of three laser sensors, scanning eight transects spaced 600 m along the sensor acquisition range. Each transect collects waveforms at 25 m radial footprints every 60 m along the track direction, with a geolocation error lower than 8 m in X/Y coordinates and 10 cm in Z. The GEDI science team derived tree height subtracting the highest return (first received return) and the elevation, interpreted as the mode of the lowest value in the received waveform (Figure ED1). We used the Level 2 A product, including footprint-level elevation and relative canopy heights (RH)—referred to as the height above the ground of each energy percentile along the waveform profile-. To minimize noise in canopy height detection, we selected only high-quality footprints (quality flag = 1) collected during nighttime, and with a sensitivity greater than 0.97, as recommended by the GEDI science team[54]. To open and process the GEDI data, we used the "rGEDI" R package[55].

It is worth noting that GEDI tends to overestimate tree heights in mountainous areas[50]. Therefore, we applied a sequence of filters to reduce signal noise and minimize overestimation. Firstly, we restricted the analysis domain to mountain forests, i.e., locations higher than 800 m according to the FAO criteria[51]. Since noise is concentrated in the upper lands (due to steep slopes and snow cover[50,56,57]), we determined the treeline excluding the top 0.1% footprints of each mountain range to cleanse the upper tail of the distribution, where the signal consists mostly of outliers and detection errors (Figure SI2 exemplifies the procedure). Then, we applied an outlier filter along the entire elevation gradient. We grouped GEDI's footprints into 50 m interval classes of elevation. Within each 50 m interval, we retained only those footprints falling within the interval's mean of the tree height (RH95 – tree height observed at 95 quantiles of the returned energy) ± 3 standard deviations[58]. After quality control and noise reduction filtering processes, a total of 780,314 footprints remained.

To retrieve the maximum tree height along gradients of explanatory variables, we retained only those footprints with tree heights between the 90th and 95th percentiles of RH95 in each 25 m elevation interval between 800 m and the estimated treeline. Temperature and precipitation data were subjected to the same maximum tree height estimation procedure. For this, we defined interval classes to cleanse noise and calculate maximum height using the same number of intervals estimated during elevation noise removal and maximum tree height estimation procedures (remaining 38,883). We adapted the interval size to obtain approximately the same number of classes obtained in the case of elevation.

Ancillary data

Since GEDI provides the baseline for calculating relative heights and not the actual elevation of the ground, elevation data were retrieved from the NASADEM_HGT digital elevation model (DEM), a 30 m spatial resolution enhancement of the former STRM DEM with improved accuracy by incorporating data from SAR, LiDAR and optical sensors[59]. Climate data were retrieved from the WorldClim 2.1[28] climate dataset. We extracted historical (1970–2000) information about seasonal and annual minimum temperature (Tmin), maximum temperature (Tmax), and Precipitation (Prec), at a spatial resolution of 30 arc seconds (0.65 km at latitude 45°). From this data, we derived a set of climate variables with potential physiological effects on tree growth and development, based on the literature[15]: (i) length of growing season (LGS), corresponding to the days without tree growing restrictions (see description below); (ii) average minimum temperature during the growth season ($T_{MeanMinGS}$); (iii) average summer maximum temperature ($T_{MeanMaxSummer}$); (iv) annual precipitation ($Prec_{AccAnnual}$) and (v) summer precipitation ($Prec_{AccSummer}$). In the case of LGS and $T_{MeanMinGS}$, we transformed the monthly average and minimum temperatures into mean and minimum daily temperatures by means of cubic splines interpolation[15], using stats R package. Then, we defined the growing season as the annual count of days between the first span of at least 6 consecutive days with mean temperature >5 °C and the first span—after July—of 6 days with mean temperature <5 °C, following the Expert Team on Climate Change Detection and Indices (ETCCDI)[60].

Modeling approach

After filtering the data, we ran a series of regression models to assess the strength and shape of the relationship between maximum tree height, elevation, and climatic variables. For this purpose, we tested log-linear (Eq. (1)), segmented (Eq. (2)), and Gaussian (Eq. (3)) univariate models for each candidate predictor (see previous section). We chose these model formulations based on observed data patterns during exploratory analyses. Segmented models were parameterized by searching for the optimal number of breakpoints through a subsampling method, running 50 iterations with 5 folds, using the segmented R package[61]. Log-linear and Gaussian models were adjusted following Eqs. 1 and 3 using the "stats" R package. To avoid potential misspecification of the model due to spatial autocorrelation, we fitted 1000 models for each variable and model formulation. In each iteration, we randomly retained half of the dataset as the training dataset and the other half as test subsamples. We then calculated the median and standard deviation of all parameter estimates across the 1000 repetitions. In the case of segmented models, we also retrieved the median and the standard deviation of the breakpoint position and the slope below and above the breakpoint. We computed the R-squared (R^2) and root mean standard error (RMSE) – calculated using the validation sample – as indicators of model performance, using the metrics R package[62].

$$\log(max.tree\ height) = \alpha_1 + \beta_1 \cdot x \tag{1}$$

Where $\alpha 1$ is the intercept, $\beta 1$ is the slope, and x is the predictor of maximum tree height.

$$\log(max.tree\ height) = \begin{cases} \alpha_1 + \beta_1 \cdot x \,\forall x \le \Psi \\ \alpha_2 + \beta_2 \cdot x \,\forall x > \Psi \end{cases} \tag{2}$$

Where $\alpha 1$ and $\alpha 2$ are the intercepts, $\beta 1$ and $\beta 2$ are the slopes of the relationship above and below the breakpoint, respectively, while ψ is the breakpoint.

$$\max .tree\ height = H\,max \times exp\left[-\frac{1}{2}\left(\frac{x-a}{b}\right)\right]^2 \tag{3}$$

Where a, b, and H_{max} are parameters estimated by the model. a represents the value of x at which the maximum tree height reaches the highest value, whereas b controls for the width of the curve.

Climate change effects on tree height development

To assess the connection between climate variables and elevation, we derived isohyets, isotherms, and isolines based on the breakpoints identified for the relationship between maximum tree height and precipitation, temperature, or other variables, respectively. We then extracted elevation values corresponding to these isolines, and we evaluated and plotted the distance between elevation breakpoints derived from climate variables and those estimated using DEM and GEDI data. This method allows us to analyze the relationship between climate parameters and elevation.

The effect exerted by climate change on the position of the elevation breakpoint was assessed by forecasting the position of the climatic

breakpoints for the Shared Socioeconomic Pathways (SSPs) 245 (CO_2 emissions around current levels until 2050, then falling but not reaching net zero by 2100) and 585 (CO_2 emissions triple by 2075). We retrieved spatial predictions of $T_{MeanMaxSummer}$ in the period 2080–2100 based on the ensemble predictions from eight general circulation models (GCMs): BCC-CSM2-MR[63], CNRM-CM6-1[64], CNRM-ESM2-1[65], CanESM5[66], IPSL-CM6A-LR[67], MIROC-ES2L[68], MIROC6[69], MRI-ESM2-0[70] under the scenarios SSP245 and SSP585. We then shifted the position of the breakpoint according to future climatic conditions, moving it upwards at a rate of 100 m.a.s.l. for each 0.65 C° increase in $T_{MeanMaxSummer}$ with respect to current conditions at the breakpoint.

Since the dynamics of the treeline are likely to follow different patterns and have been proven to present great inertia, we opted for a conservative approach, and the upward displacement of the breakpoint was restrained to the current position of the treeline. Thus, if climate scenarios predicted that the breakpoint position would be located above the current treeline, we placed it at the treeline, never above it. We used the *terra*[71] and *tidyverse*[72] R packages to manage all raster and tabulated data.

Data availability

The dataset associated with this paper comprises GEDI 2A data collected from 2019/05/01 to 2020/09/03, along with ancillary data (NASADEM & WorldClim) at the footprint level. Additionally, footprints are filtered by elevation ranging from 800 meters above sea level to the maximum elevation calculated for each mountain range (please see Methods/GEDI Dataset subsection). Each file encompasses the described data for a specific mountain range (specified in the filename) and is presented as a *.RData file. This data is prepared for modeling and plotting and is accessible at: https://doi.org/10.5281/zenodo.10490202.

Received: 4 July 2023; Accepted: 30 January 2024;
Published online: 15 February 2024

References

1. Price, M., Gratzer, G., Alemayehu Duguma, L., Kohler, T. & Maselli, D. Mountain forests in a changing world: realizing values, adressing challenges. (FAO/MPS and SDC, 2011).
2. UNESCO. Mountain ecosystem services and climate change: a global overview of potential threats and strategies for adaptation. (2017).
3. Albrich, K., Rammer, W. & Seidl, R. Climate change causes critical transitions and irreversible alterations of mountain forests. *Glob. Change Biol.* **26**, 4013–4027 (2020).
4. Grace, J., Berninger, F. & Nagy, L. Impacts of climate change on the tree line. *Ann. Bot.* **90**, 537–544 (2002).
5. Silva, C. A. et al. Comparison of small- and large-footprint lidar characterization of tropical forest aboveground structure and biomass: a case study from central gabon. *IEEE J. Select. Top. Appl. Earth Obs. Remote Sens.* **11**, 3512–3526 (2018).
6. Qi, W., Saarela, S., Armston, J., Ståhl, G. & Dubayah, R. Forest biomass estimation over three distinct forest types using TanDEM-X InSAR data and simulated GEDI lidar data. *Remote Sens. Environ.* **232**, 111283 (2019).
7. Cazzolla Gatti, R., Di Paola, A., Bombelli, A., Noce, S. & Valentini, R. Exploring the relationship between canopy height and terrestrial plant diversity. *Plant Ecol.* **218**, 899–908 (2017).
8. Lopatin, J., Dolos, K., Hernández, H. J., Galleguillos, M. & Fassnacht, F. E. Comparing generalized linear models and random forest to model vascular plant species richness using LiDAR data in a natural forest in central Chile. *Remote Sens. Environ.* **173**, 200–210 (2016).
9. Zhang, J., Nielsen, S. E., Mao, L., Chen, S. & Svenning, J.-C. Regional and historical factors supplement current climate in shaping global forest canopy height. *J. Ecol.* **104**, 469–478 (2016).
10. Cramer, M. D. Unravelling the limits to tree height: a major role for water and nutrient trade-offs. *Oecologia* **169**, 61–72 (2011).
11. McDowell, N. G. et al. Pervasive shifts in forest dynamics in a changing world. *Science* **368**, eaaz9463 (2020).
12. Ellis, E. C. et al. People have shaped most of terrestrial nature for at least 12,000 years. *Proc. Natl. Acad. Sci.* **118**, e2023483118 (2021).
13. Kašpar, J., Tumajer, J., Šamonil, P. & Vašíčková, I. Species-specific climate–growth interactions determine tree species dynamics in mixed Central European mountain forests. *Environ. Res. Lett.* **16**, 034039 (2021).
14. Körner, C. & Paulsen, J. A world-wide study of high altitude treeline temperatures. *J. Biogeogr.* **31**, 713–732 (2004).
15. Paulsen, J. & Körner, C. A climate-based model to predict potential treeline position around the globe. *Alp. Bot.* **124**, 1–12 (2014).
16. Campbell, E. M., Magnussen, S., Antos, J. A. & Parish, R. Size-, species-, and site-specific tree growth responses to climate variability in old-growth subalpine forests. *Ecosphere* **12**, e03529 (2021).
17. Fricker, G. A. et al. More than climate? Predictors of tree canopy height vary with scale in complex terrain, Sierra Nevada, CA (USA). *Forest Ecol. Manag.t* **434**, 142–153 (2019).
18. Frenne, P. D. et al. Forest microclimates and climate change: Importance, drivers and future research agenda. *Glob. Change Biol.* **27**, 2279–2297 (2021).
19. Messaoud, Y. & Chen, H. Y. H. The influence of recent climate change on tree height growth differs with species and spatial environment. *PLoS One* **6**, e14691 (2011).
20. Larjavaara, M. & Muller-Landau, H. C. Measuring tree height: a quantitative comparison of two common field methods in a moist tropical forest. *Methods Ecol. Evol.* **4**, 793–801 (2013).
21. Valbuena, R. et al. Standardizing ecosystem morphological traits from 3D information sources. *Trends Ecol. Evol.* **35**, 656–667 (2020).
22. Wulder, M. A. et al. Lidar sampling for large-area forest characterization: a review. *Remote Sens. Environ.* **121**, 196–209 (2012).
23. Hancock, S., McGrath, C., Lowe, C., Davenport, I. & Woodhouse, I. Requirements for a global lidar system: spaceborne lidar with wall-to-wall coverage. *R. Soc. Open Sci.* **8**, 211166 (2021).
24. Schneider, F. D. et al. Towards mapping the diversity of canopy structure from space with GEDI. *Environ. Res. Lett.* **15**, 115006 (2020).
25. Ameztegui, A., Rodrigues, M., Gelabert, P., Lavaquiol, B. & Coll, L. Maximum height of mountain forests abruptly decreases above an elevation breakpoint. *GISci. Remote Sens.* **58**, 442–454 (2021).
26. Coops, N. C., Morsdorf, F., Schaepman, M. E. & Zimmermann, N. E. Characterization of an alpine tree line using airborne LiDAR data and physiological modeling. *Glob. Change Biol.* **19**, 3808–3821 (2013).
27. Mandl, L., Stritih, A., Seidl, R., Ginzler, C. & Senf, C. Spaceborne LiDAR for characterizing forest structure across scales in the European Alps. *Remote Sens. Ecol. Conserv*. https://doi.org/10.1002/rse2.330 (2023).
28. Fick, S. E. & Hijmans, R. J. WorldClim 2: new 1-km spatial resolution climate surfaces for global land areas. *Int. J. Climatol.* **37**, 4302–4315 (2017).
29. Gonzalez-Hidalgo, J. C., Peña-Angulo, D., Beguería, S. & Brunetti, M. MOTEDAS century: A new high-resolution secular monthly maximum and minimum temperature grid for the Spanish mainland (1916–2015). *Int. J. Climatol.* **40**, 5308–5328 (2020).
30. Tao, S., Guo, Q., Li, C., Wang, Z. & Fang, J. Global patterns and determinants of forest canopy height. *Ecology* **97**, 3265–3270 (2016).
31. Körner, C. Alpine treelines: functional ecology of the global high elevation tree limits. (Springer Science & Business Media, 2012).
32. Holtmeier, F.-K. & Broll, G. Wind as an ecological agent at treelines in North America, the Alps, and the European Subarctic. *Phys. Geogr.* **31**, 203–233 (2010).
33. Seidl, R., Rammer, W. & Blennow, K. Simulating wind disturbance impacts on forest landscapes: tree-level heterogeneity matters. *Environ. Model. Softw*. **51**, 1–11 (2014).

34. Doležal, J. & Šrůtek, M. Altitudinal changes in composition and structure of mountain-temperate vegetation: a case study from the Western Carpathians. *Plant Ecol.* **158**, 201–221 (2002).
35. Klein, T., Randin, C. & Körner, C. Water availability predicts forest canopy height at the global scale. *Ecol. Lett.* **18**, 1311–1320 (2015).
36. Zhang, B. & Yao, Y. Implications of mass elevation effect for the altitudinal patterns of global ecology. *J. Geogr. Sci.* **26**, 871–877 (2016).
37. Elsen, P. R., Monahan, W. B. & Merenlender, A. M. Topography and human pressure in mountain ranges alter expected species responses to climate change. *Nat. Commun.* **11**, 1974 (2020).
38. Pau, M. et al. Site index as a predictor of the effect of climate warming on boreal tree growth. *Glob. Change Biol.* **28**, 1903–1918 (2021).
39. Lloyd, A. H., Sullivan, P. F. & Bunn, A. G. Integrating dendroecology with other disciplines improves understanding of upper and latitudinal treelines. *In:* Dendroecology: Tree-Ring Analyses Applied to Ecological Studies (eds. Amoroso, M. M., Daniels, L. D., Baker, P. J. & Camarero, J. J.) 135–157. https://doi.org/10.1007/978-3-319-61669-8_6 (Springer International Publishing, 2017).
40. Wilmking, M. & Juday, G. P. Longitudinal variation of radial growth at Alaska's northern treeline—recent changes and possible scenarios for the 21st century. *Glob. Planet. Change* **47**, 282–300 (2005).
41. Henttonen, H. M., Nöjd, P. & Mäkinen, H. Environment-induced growth changes in the Finnish forests during 1971–2010 – an analysis based on National Forest Inventory. *Forest Ecol. Manag.* **386**, 22–36 (2017).
42. Hilmers, T. et al. The productivity of mixed mountain forests comprised of Fagus sylvatica, Picea abies, and Abies alba across Europe. *Forestry* **92**, 512–522 (2019).
43. Härkönen, S. et al. A climate-sensitive forest model for assessing impacts of forest management in Europe. *Environ. Model. Softw.* **115**, 128–143 (2019).
44. Mina, M. et al. Future ecosystem services from European mountain forests under climate change. *J. Appl. Ecol.* **54**, 389–401 (2017).
45. Barnaud, C. et al. Is forest regeneration good for biodiversity? Exploring the social dimensions of an apparently ecological debate. *Environ. Sci. Policy* **120**, 63–72 (2021).
46. Hansson, A., Dargusch, P. & Shulmeister, J. A review of modern treeline migration, the factors controlling it and the implications for carbon storage. *J. Mt. Sci.* **18**, 291–306 (2021).
47. Stritih, A., Seidl, R. & Senf, C. Alternative states in the structure of mountain forests across the Alps and the role of disturbance and recovery. *Landsc. Ecol.* **38**, 933–947 (2023).
48. Roy, D. P., Kashongwe, H. B. & Armston, J. The impact of geolocation uncertainty on GEDI tropical forest canopy height estimation and change monitoring. *Sci. Remote Sens.* **4**, 100024 (2021).
49. Kutchartt, E., Pedron, M. & Pirotti, F. Assessment of canopy and ground height accuracy from gedi lidar over steep mountain areas. *ISPRS Annals of the Photogrammetry, Remote Sensing and Spatial Information Sciences* **V-3–2022**, 431–438 (2022).
50. Potapov, P. et al. Mapping global forest canopy height through integration of GEDI and Landsat data. *Remote Sens. Environ.* **253**, 112165 (2021).
51. FAO. Global ecological Zones for FAO forest reporting: 2010 update. https://www.fao.org/documents/card/en?details=c4ce1aec-7b11-516e-a9c0-ca2ee01b505d/ (2012).
52. Dubayah, R. et al. GEDI L2A elevation and height metrics data global footprint level V001 [Data set]. NASA EOSDIS Land Processes DAAC https://doi.org/10.5067/GEDI/GEDI02_A.001 (2020).
53. Dubayah, R. et al. The global ecosystem dynamics investigation: high-resolution laser ranging of the Earth's forests and topography. *Sci. Remote Sens.* https://doi.org/10.1016/j.srs.2020.100002 (2020).
54. Beck, J., Armston, J., Hofton, M. & Luthcke, S. Global ecosystem dynamics investigation (GEDI) level 02 user guide. (EROS Center, U.S. Geological Survey, 2020).
55. Silva, C. A. et al. rGEDI: NASA's global ecosystem dynamics investigation (GEDI) data visualization and processing. version 0.1.9, https://github.com/carlos-alberto-silva/rGEDI.
56. Hancock, S. et al. The GEDI simulator: a large-footprint waveform lidar simulator for calibration and validation of spaceborne missions. *Earth Space Sci.* **6**, 294–310 (2019).
57. Qi, W. et al. Improved forest height estimation by fusion of simulated GEDI Lidar data and TanDEM-X InSAR data. *Remote Sens. Environ.* **221**, 621–634 (2019).
58. Zhao, Y., Lehman, B., Ball, R., Mosesian, J. & de Palma, J.-F. Outlier detection rules for fault detection in solar photovoltaic arrays. in 2013 Twenty-Eighth Annual IEEE Applied Power Electronics Conference and Exposition (APEC) 2913–2920 https://doi.org/10.1109/APEC.2013.6520712 (2013).
59. NASA JPL. NASADEM Merged DEM Global 1 arc second V001 [Data set]. NASA EOSDIS Land Processes DAAC. https://doi.org/10.5067/MEaSUREs/NASADEM/NASADEM_HGT.001 (2020).
60. Zhang, X. et al. Indices for monitoring changes in extremes based on daily temperature and precipitation data. *Wiley Interdiscip. Rev. Clim. Change* **2**, 851–870 (2011).
61. Muggeo, V. M. R. segmented: an R package to fit regression models with broken-line relationships. *R News* **8**, 20–25 (2008).
62. Hamner, B. & Frasco, M. Metrics: evaluation metrics for machine learning. (2018).
63. Wu, T. et al. BCC-CSM2-HR: a high-resolution version of the Beijing climate center climate system model. *Geosci. Model Dev.* **14**, 2977–3006 (2021).
64. Voldoire, A. et al. Evaluation of CMIP6 DECK Experiments With CNRM-CM6-1. *J. Adv. Model. Earth Syst.* **11**, 2177–2213 (2019).
65. Séférian, R. et al. Evaluation of CNRM earth system model, CNRM-ESM2-1: role of earth system processes in present-day and future climate. *J. Adv. Model. Earth Syst.* **11**, 4182–4227 (2019).
66. Swart, N. C. et al. The Canadian earth system model version 5 (CanESM5.0.3). *Geosci. Model Dev.* **12**, 4823–4873 (2019).
67. Boucher, O. et al. Presentation and evaluation of the IPSL-CM6A-LR climate model. *J. Adv. Model. Earth Syst.* **12**, e2019MS002010 (2020).
68. Hajima, T. et al. Development of the MIROC-ES2L Earth system model and the evaluation of biogeochemical processes and feedbacks. *Geosci. Model Dev.* **13**, 2197–2244 (2020).
69. Tatebe, H. et al. Description and basic evaluation of simulated mean state, internal variability, and climate sensitivity in MIROC6. *Geosci. Model Dev.* **12**, 2727–2765 (2019).
70. Yukimoto, S. et al. The meteorological research institute earth system model version 2.0, MRI-ESM2.0: description and basic evaluation of the physical component. *J. Meteorol. Soc. Jpn Ser. II* **97**, 931–965 (2019).
71. Hijmans, R. J. terra: spatial data analysis. (2023).
72. Wickham, H. et al. Welcome to the tidyverse. *J. Open Source Softw.* **4**, 1686 (2019).

Acknowledgements

This study has been supported by the Catalan Agency for Management of University and Research Grants (ADAPTAFOR, 2021-SGR-01530). AA is a Serra-Hunter fellow funded by the Generalitat de Catalunya.

Author contributions

PG: conceptualization, methodology, data curation, formal analysis, writing—original draft; MR: conceptualization, methodology, writing—review & editing; LC: conceptualization, methodology, writing—review & editing; CV: conceptualization, writing—review & editing; AA: supervision, conceptualization, methodology, writing—review & editing.

Competing interests

The authors declare no competing interests.

Additional information

Supplementary information The online version contains supplementary material available at https://doi.org/10.1038/s43247-024-01246-5.

Correspondence and requests for materials should be addressed to P. J. Gelabert.

Peer review information *Communications Earth & Environment* thanks the anonymous reviewers for their contribution to the peer review of this work. Primary Handling Editor: Aliénor Lavergne. A peer review file is available.